JOBNAME: JCLI 21#21 2008 PAGE: 1 SESS: 8 OUTPUT: Sat Dec 6 06:24:33 2008 Total No. of Pages: 15
/ams/jcli/170147/jcli2505





# The Dynamical Response to Snow Cover Perturbations in a Large Ensemble of Atmospheric GCM Integrations

CHRISTOPHER G. FLETCHER, STEVEN C. HARDIMAN, AND PAUL J. KUSHNER

*Department of Physics, University of Toronto, Toronto, Ontario, Canada*

JUDAH COHEN

*AER, Inc., Lexington, Massachusetts*

(Manuscript received 3 March 2008, in final form 25 July 2008)

ABSTRACT

Variability in the extent of fall season snow cover over the Eurasian sector has been linked in observations to a teleconnection with the winter northern annular mode pattern. Here, the dynamics of this teleconnection are investigated using a 100-member ensemble of transient integrations with the GFDL atmospheric general circulation model (AM2). The model is perturbed with a simple persisted snow anomaly over Siberia and is integrated from October through December. Strong surface cooling occurs above the anomalous Siberian snow cover, which produces a tropospheric form stress anomaly associated with the vertical propagation of wave activity. This wave activity response drives wave-mean flow interaction in the lower stratosphere and subsequent downward propagation of a negative-phase northern annular mode response back into the troposphere. A wintertime coupled stratosphere–troposphere response to fall season snow forcing is also found to occur even when the snow forcing itself does not persist into winter. Finally, the response to snow forcing is compared in versions of the same model with and without a well-resolved stratosphere. The version with the well-resolved stratosphere exhibits a faster and weaker response to snow forcing, and this difference is tied to the unrealistic representation of the unforced lower-stratospheric circulation in that model.

## 1. Introduction

Snow cover is a highly variable land surface condition that exerts a strong control on the heat and moisture budget of the overlying atmosphere (Cohen and Rind 1991; Vavrus 2007). However, recent work has shown that regional snow cover variability can also lead to remote and even hemispheric-scale circulation responses. The most studied teleconnection is between variations in fall season Siberian snow cover and lagged changes in the winter northern annular mode (NAM; Thompson and Wallace 2000) pattern (Cohen and Entekhabi 1999; Gong et al. 2003; Cohen et al. 2007; Cohen and Fletcher 2007). For example, an early snowfall over Siberia leads to a zonally asymmetric surface forcing that excites a Rossby wave activity pulse (Cohen et al. 2007). The Rossby wave activity that is absorbed in the stratosphere weakens the polar vortex and warms the polar stratosphere. This zonal circulation response, which projects onto the negative phase of the NAM, propagates downward in the following weeks and sets up a negative NAM anomaly in the troposphere (Baldwin and Dunkerton 2001).

The observed tropospheric NAM signals associated with October snow anomalies peak in January (Cohen et al. 2007). This 3-month separation is associated with significant seasonal predictability (Cohen and Fletcher 2007). However, because the lagged correlations between the two signals have a magnitude of about 0.5, there has been some debate about the dynamical and statistical robustness of the link (Limpasuvan et al. 2005; Kushnir et al. 2006). It seems clear that once the stratosphere is in a strong anomalous NAM phase, Baldwin and Dunkerton (2001)-type downward propagation of the NAM signal into the troposphere will often occur. This provides the potential for using stratospheric NAM anomalies to be used as wintertime surface circulation

*Corresponding author address:* Christopher G. Fletcher, Department of Physics, University of Toronto, 60 St. George St., Toronto, M5S 1A7, Canada.
E-mail: chris.fletcher@utoronto.ca

DOI: 10.1175/2008JCLI2505.1

JOBNAME: JCLI 21#21 2008 PAGE: 2 SESS: 8 OUTPUT: Sat Dec 6 06:24:33 2008 Total No. of Pages: 15
/ams/jcli/170147/jcli2505





predictors (Baldwin et al. 2003; Charlton et al. 2004; Siegmund 2005). Our key interest is to characterize the snow-forced teleconnection and to see if it is a reliable precursor to the stratospheric NAM anomaly.

This work will present three principal results. First, after describing our modeling approach (section 2), we demonstrate that strong surface cooling associated with anomalous Siberian snow cover can produce a large-scale Rossby wave response that drives wave-mean flow interaction in the lower stratosphere through the generation of long baroclinic eddies and Eliassen–Palm (EP) fluxes (section 3a). Second, we show that it is possible to initiate a wintertime coupled stratosphere–troposphere response to fall season snow forcing even when the snow forcing itself does not persist through the entire winter (section 3b). Third, we compare the response in a general circulation model (GCM) with a well-resolved stratosphere (''high-top GCM'') to that in a more standard GCM with poor stratospheric representation (''low-top GCM''). We find that the high-top GCM has a faster and weaker response to snow forcing than the low-top GCM, and that this difference is tied to the unrealistic representation of the high-top model's lower-stratospheric circulation (section 4). We believe that these findings present a significant advance in the understanding of the transient dynamical response of the coupled stratosphere–troposphere system to mid-latitude surface forcing and provide increased potential for seasonal climate forecasting in the extratropics.

## 2. Methods

### a. Model description

We use the Geophysical Fluid Dynamics Laboratory (GFDL) atmospheric GCM (AM2)/land GCM (LM2; Anderson et al. 2004), which is the atmospheric component of the coupled ocean–atmosphere Climate Model version 2.1 (CM2.1) described in Delworth et al. (2006) and used for climate and seasonal prediction studies at GFDL. The atmospheric model uses the finite-volume dynamical core with terrain-following Lagrangian control-volume discretization, as described in Lin (2004). The model horizontal resolution is 2° latitude × 2.5° longitude. The land surface component, LM2, is relatively simple, but it is adequate for the prescribed snow perturbations we use for this study.

We are interested in how a GCM's stratospheric representation affects the response to surface forcing (Kushner et al. 2007). The Fletcher et al. (2007) analysis used the standard version of the GFDL AM2/LM2, which has a relatively poorly resolved stratosphere. This low-top version will be called AM2-LO. In this study, we also analyze an ensemble of integrations using a model with improved stratospheric representation (''AM2-HI''). AM2-LO is run with 24 vertical layers (4 layers above 100 hPa) and a model lid situated in the upper stratosphere at 3 hPa (~45 km). The top layer of the model is a sponge layer, where Rayleigh friction damps anomalies in the zonal mean zonal wind on a time scale of 40 days. The Rayleigh drag scheme is numerically simple but physically inconsistent because it may introduce spurious vertically coupled circulation responses (Shepherd et al. 1996; Shepherd and Shaw 2004)

AM2-HI is a nonchemistry version of the coupled chemistry climate model employed in Austin and Wilson (2006). It is run with 48 vertical layers (21 layers above 100 hPa) and a model lid height in the upper mesosphere at 0.003 hPa (~100 km). In AM2-HI, the Rayleigh friction sponge layer is replaced with the nonorographic gravity wave drag (GWD) scheme described by Alexander and Dunkerton (1999). Orographic gravity waves above 30 hPa are fluxed to space rather than being absorbed by the zonal mean circulation. A comparison between the responses to snow forcing in AM2-LO and AM2-HI is provided in section 4a.

### b. Snow perturbation method

Following Fletcher et al. (2007) we investigate the transient atmospheric circulation response to a switch-on snow perturbation during fall. The time of the transition to snow-covered conditions in the Siberian region varies greatly from year to year (Robinson et al. 1993). In a simple way our snow perturbation experiment represents an early start to the snow season in this region. To obtain robust statistics we use a 100-member ensemble of realizations started from independent initial conditions. Each ensemble member is initialized from a 100-yr simulation of GFDL AM2/LM2 forced with observed climatological sea surface temperatures and sea ice and fixed atmospheric composition (hereafter ''unforced control run'').

Every 1 October of this 100-yr unforced control run, we branch two additional simulations that run from 1 October to 31 December. In the first set of branch simulations, we hold the snow mass field fixed throughout the run at its 1 October value at each land surface point (hereafter LOW-SNOW). In the AM2-LO climatology (not shown) less than 10% of the land area of Eurasia is snow covered on October 1 and the majority of this area lies poleward of 60°N.

The second set of branch simulations are the same, except we add to the 1 October snow mass field a 100 kg $m^{-2}$ perturbation over the Siberia region 40°–80°N, 60°–140°E (hereafter HIGH-SNOW, see Fig. 1a). F1

JOBNAME: JCLI 21#21 2008 PAGE: 3 SESS: 8 OUTPUT: Sat Dec 6 06:24:33 2008 Total No. of Pages: 15
/ams/jcli/170147/jcli2505





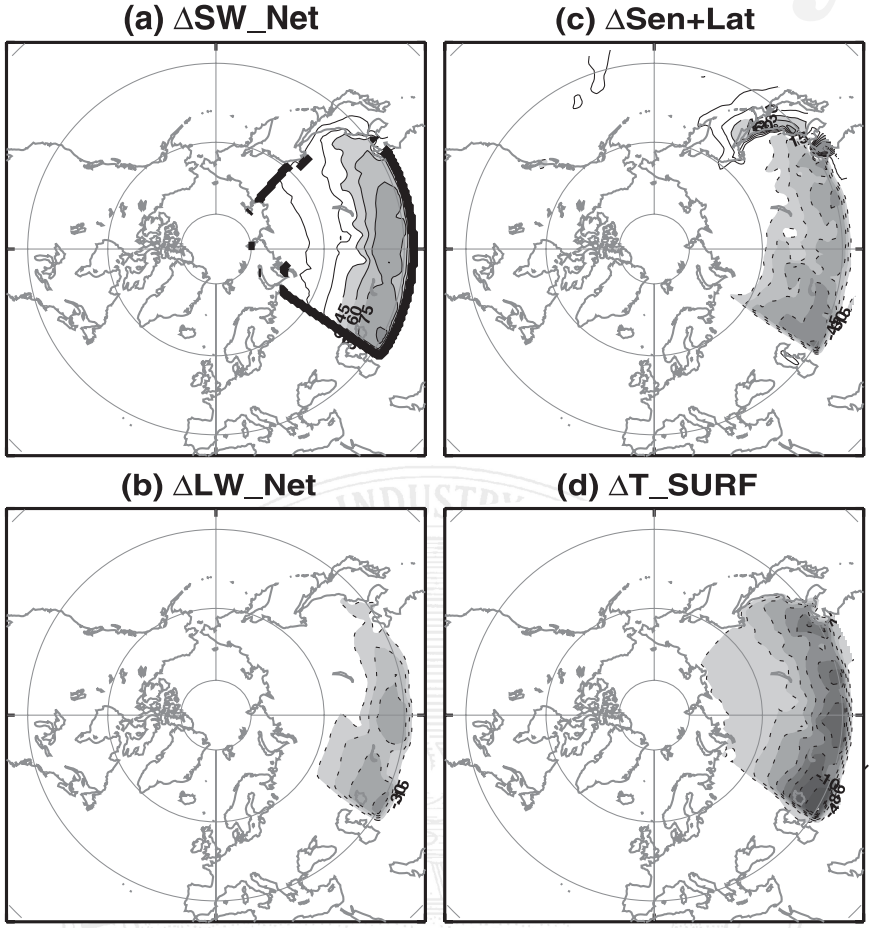


FIG. 1. Time-averaged ensemble mean surface response to snow forcing for days 1–15 in (a) net shortwave radiation (W $m^{-2}$), (b) net longwave radiation (W $m^{-2}$), (c) sensible plus latent turbulent heat fluxes (W $m^{-2}$), and (d) surface temperature (K). Contour interval and shading (a)–(c) is 15 W $m^{-2}$ and in (d) is 2 K, and negative contours are dashed. All contours shown are statistically significant (see section 2b for details). Positive values (a)–(c) indicate upward fluxes. Thick black line in (a) indicates the boundary of the snow perturbation.

Assuming a representative snow density of 250 kg $m^{-3}$ (Frei et al. 2003), the perturbation is equivalent to a 0.4-m-deep snow layer, which is characteristic of a midwinter value. We have verified (not shown) that our results are insensitive to varying this depth between 0.04 and 4 m. The spatial extent of snow cover is therefore the dominant forcing parameter, which over the perturbation region is equivalent to the climatological January extent in AM2-LO.

At each time step our snow perturbation is applied by resetting the model-derived snow mass to our prescribed snow mass value (100 kg $m^{-2}$). Snow is allowed to fall and accumulate at the surface as normal, and melting of existing snow mass can occur, releasing latent heat to the atmosphere and soil moisture to the land model. Water and energy are therefore not conserved during each realization. However, we have found (not shown) that similar, albeit weaker, responses are obtained if the snow perturbation is allowed to melt away, rather than being held fixed, after it is prescribed on day 1. Once switched on, the snow perturbation is held constant throughout each branch run and the forcing comes from the Siberia region alone. We will show in section 3 that the impact of the snow perturbation on the atmosphere is primarily due to the increased surface albedo associated with the greater snow areal extent. We would therefore expect a similar response if we altered the surface albedo directly; however, in our model this procedure was more computationally challenging than fixing the snow mass.

For a given field $\mathbf{X}$ we define the response to the snow perturbation in a single realization as

$$\Delta\mathbf{X} = \mathbf{X}_{\text{HIGH\_SNOW}} - \mathbf{X}_{\text{LOW\_SNOW}}. \quad (1)$$

The statistical significance of the time-evolving response is assessed for each simulation day using the one-sample Student's $t$ test (Wilks 2006)

$$t = \frac{\langle \Delta \mathbf{X} \rangle - \mu_0}{[\widehat{\mathrm{Var}}\langle \Delta \mathbf{X} \rangle]^{1/2}}, \tag{2}$$

where $\langle \Delta \mathbf{X} \rangle$ denotes the ensemble mean response, $\mu_0$ is the mean of the null hypothesis ($H_0$), and $\widehat{\mathrm{Var}}\langle \Delta \mathbf{X} \rangle$ is the variance of the sampling distribution ($s^2$) divided by $n$, where $n = 100$ is the number of realizations. We find that the individual ensemble realizations diverge from each other as a monotonic function of time, so that $\widehat{\mathrm{Var}}\langle \Delta \mathbf{X} \rangle$ is significantly larger on 31 December than on 1 October. However, this statistical test is appropriate if we make the safe assumption that the ensemble of realizations, starting at 1-yr intervals from a long climatological SST integration, is independent and identically distributed for each simulation day. The null hypothesis ($H_0$) is that there is no systematic response to snow forcing; that is, we specify $H_0$ such that $\langle \Delta \mathbf{X} \rangle = \mu_0 = 0$. A significant response is found when $t > t_c$, where $t_c$ is the critical value of $t$ for $n = 100$ at a significance level of 0.05. This allows for a 5% chance of incorrectly rejecting $H_0$. For time-averaged quantities, the $t$ test is computed using the time-averaged fields.

## 3. Transient response to Siberian snow forcing

### *a. Phases of the transient response in AM2-LO*

The dominant effect of the snow perturbation is to increase the surface albedo over the perturbation region from ~0.15 to ~0.65 (see Fletcher et al. 2007, their Fig. 1). We found (not shown) that effects such as longwave insulation and soil moisture anomalies from melting snow have a small impact on the seasonal time-scale atmospheric response. This is in general agreement with previous studies where GCMs were forced with snow perturbations (Cohen and Rind 1991; Gong et al. 2003).

The atmospheric response to snow forcing is driven by the increased albedo, which causes a strong radiative cooling response at the surface. Figure 1 shows the ensemble mean response in the surface radiative and turbulent fluxes during days 1–15 (1–15 October). We have calculated the area-weighted average response for each variable over the perturbation region (Fig. 1a). The snow forcing increases net (upward minus downward) surface shortwave radiation (SW) by an average of 36 W m$^{-2}$ in the snow-forcing region (Fig. 1a). Reduced SW absorption at the surface results in temperatures cooler by ~3 K (Fig. 1d) and a subsequent reduction in emitted longwave radiation of 14 W m$^{-2}$ (Fig. 1b). Turbulent fluxes of sensible and latent heat from the surface to the atmosphere are reduced by 20 W m$^{-2}$ to partially balance the SW deficit (Fig. 1c).

Following the terminology employed by Limpasuvan et al. (2004), the transient circulation response divides naturally into the following three distinct phases: (a) an onset phase (days 1–15), (b) a growth phase (days 16–65, where day 65 coincides with the peak response in the stratosphere; see below), and (c) a mature phase (days 66–92). During the onset phase, which is shown in the left column of Fig. 2, we see a Hoskins and Karoly (1981)-type baroclinic response to the Siberian region surface cooling. This response consists of a surface high (seen in the sea level pressure (SLP) response, with peak amplitude 12 hPa in Fig. 2a) situated below a free tropospheric low (seen in the 500-hPa geopotential response Fig. 2b). This regional response pattern is analogous to that of the wintertime Siberian high, which is itself maintained by snow-forced diabatic cooling (Panagiotopoulos et al. 2005). However, even in the onset phase, the response shows significant remote responses across the hemisphere. This is emphasized in Fig. 2c, where we plot the zonally asymmetric eddy component of the geopotential response at 60°N. A vertically propagating Rossby wave signal develops with an equivalent barotropic high over North America. The wave has zonal wavenumbers 1–2 and exhibits a characteristic westward phase tilt with height, indicating positive meridional eddy heat fluxes and upward propagation of Rossby wave activity (Holton 2004). In the growth phase, a pronounced teleconnected response in surface circulation develops, with low pressure centers in the North Pacific and North Atlantic (Fig. 2d). The North Pacific low in Fig. 2d extends upward and westward into the troposphere and stratosphere (Figs. 2e,f).

Our qualitative picture of the growth phase of the transient response is divided into a local diabatically forced component and a nonlocal Rossby wave dynamical component. Locally, the diabatic cooling from the snow causes isentropic surfaces to dome up. This can be seen in Fig. 3, which shows the potential temperature in the LOW-SNOW runs (solid contours) and in the HIGH-SNOW runs (dashed contours). The cooling is surface trapped, and so the doming decreases with height, leading to relatively thin (more stable) isentropic layers in the vicinity of the snow-cooled region. The nonlocal response follows from classical potential vorticity conservation arguments (Holton 2004, his section 4.3), which suggest that eastward-traveling fluid columns will develop anticylonic relative vorticity upstream of the thickness anomaly and cyclonic relative vorticity downstream of the thickness anomaly; this leads to the characteristic upstream-high/downstream-low response pattern in surface streamflow.

JOBNAME: JCLI 21#21 2008 PAGE: 5 SESS: 8 OUTPUT: Sat Dec 6 06:24:40 2008 Total No. of Pages: 15
/ams/jcli/170147/jcli2505





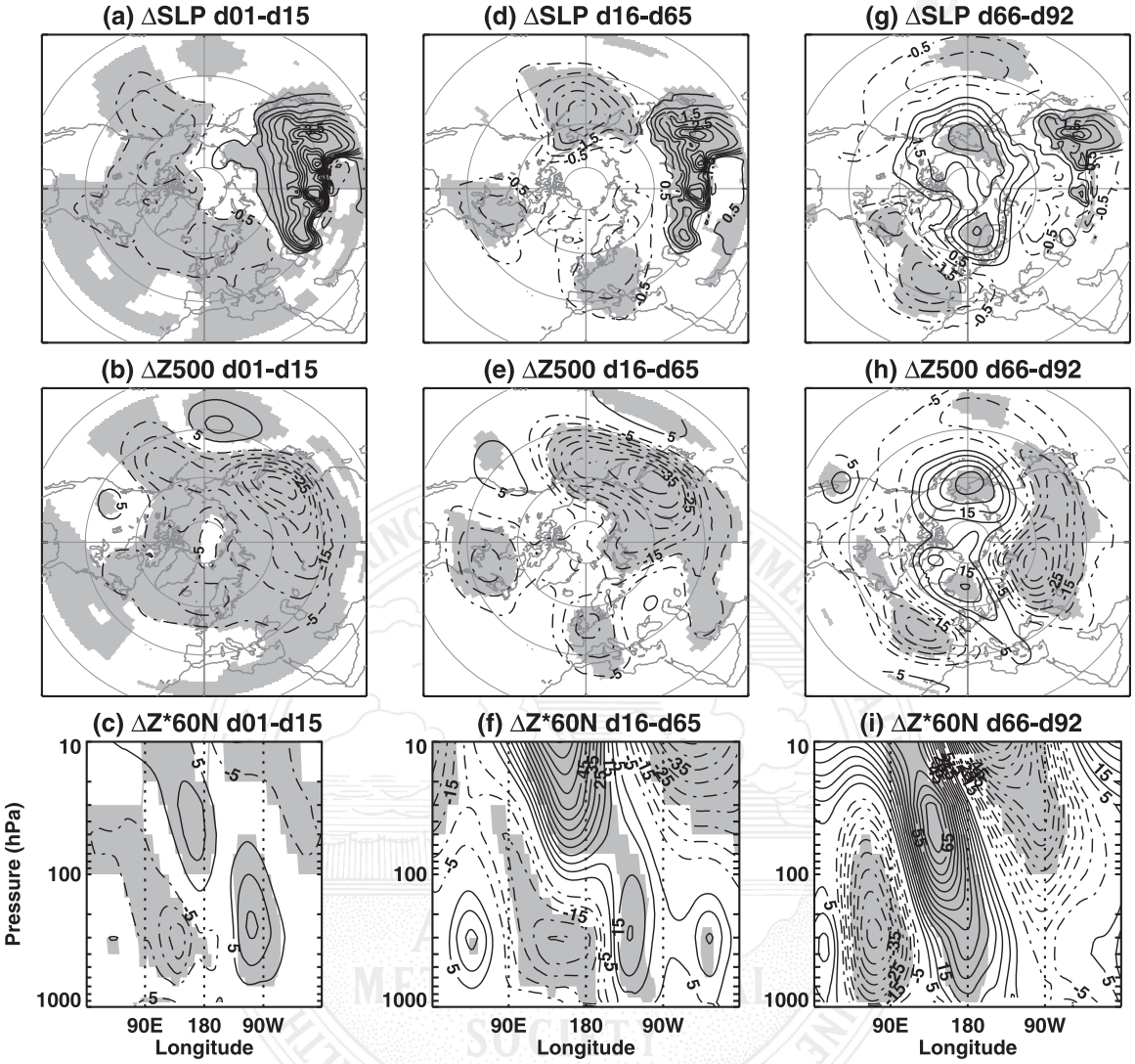


FIG. 2. Time-averaged ensemble mean response to snow forcing for (a)–(c) onset phase: days 1–15, (d)–(f) growth phase: days 16–65, and (g)–(i) mature phase: days 66–92. (a), (d), (g) Sea level pressure (ΔSLP), (b), (e), (h) geopotential height at 500 hPa ($\Delta Z500$), and (c), (f), (i) eddy geopotential height at 60°N ($\Delta Z^*60N$). Contour interval in (a), (d), (g) is 0.5 hPa and in (b), (c), (e), (f), (h), (i) is 5 m, and negative contours are dashed. Shading indicates regions of statistical significance according to a Student's *t* test (see section 2b for details).

The mature phase involves significant zonal mean and eddy components. It is characterized by an apparent negative NAM pattern (Baldwin and Dunkerton 2001) at the surface (Fig. 2g) and in the free troposphere (Fig. 2h), with an anticyclonic response over the pole and a cyclonic response in the extratropics. The wave field at 60°N still shows strong baroclinicity (Fig. 2i), although the phase has shifted westward by 90° compared to the growth phase (Fig. 2f). These results are in broad agreement with Gong et al. (2003), who showed that fall season Siberian snow forcing resulted in a significant negative NAM response at the surface during winter.

The transient response to snow forcing demonstrates that our regional snow forcing modifies the large-scale NH circulation. From the growth to the mature phase, the response develops a significant zonal component resulting from eddy-mean flow interactions. The high upstream and the low downstream of the elevated isentropic layers correspond to a positive form stress $\overline{-h'(\partial p'/\partial x)} \sim \overline{v'\theta'} > 0$, where, assuming geostrophic balance, $h'$ is the perturbation height of the isentropic surface, $\theta'$ is the perturbation potential temperature, and the overbar denotes a zonal mean (Vallis 2006, his section 7.4). The meridional heat flux $\overline{v'\theta'} > 0$ corresponds, under quasigeostrophic scaling, to an upward-propagating

JOBNAME: JCLI 21#21 2008 PAGE: 6 SESS: 8 OUTPUT: Sat Dec 6 06:24:48 2008 Total No. of Pages: 15
/ams/jcli/170147/jcli2505





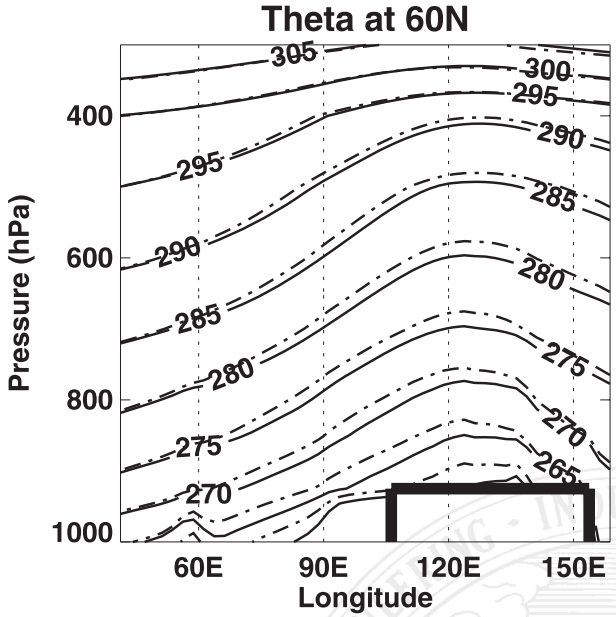


FIG. 3. Longitude–height section of potential temperature 45°–160°E at 60°N for LOW-SNOW runs (solid contours) and HIGH-SNOW runs (dashed contours). Contour interval is 5 K. Thick black line denotes values missing resulting from high topography.

EP flux (Andrews et al. 1987). Thus, the response to surface cooling serves as an anomalous source of upward-propagating Rossby wave activity for the troposphere and stratosphere.

In this study, we define the EP flux vector **F** and, hereafter, Δ**F** denotes the response in **F**, that is, the ensemble mean **F** for the HIGH-SNOW runs minus the ensemble mean **F** for the LOW-SNOW runs. In practice, we have found that Δ**F** is similar to the EP flux calculated from the ensemble mean circulation response fields. This implies that high-frequency synoptic-scale variability, that is, the weather noise present in each realization, does not produce a systematic response to the diabatic forcing. This is consistent with Gong et al. (2003) who showed that synoptic eddies are responsible for only a small fraction of the total EP flux response to snow forcing (see also Hardiman et al. 2008).

F4 Figure 4 shows the zonal mean zonal wind response ($\Delta\bar{U}$), Δ**F**, and its divergence for the three phases of the response. These zonal mean transformed Eulerian mean diagnostics (Andrews et al. 1987) are appropriate because we are interested in the interaction of snow-forced planetary waves with the mean flow. During the onset phase, $\Delta\bar{U}$ is strongest in the troposphere, with increased eastward winds at 40°N and decreased eastward winds over the polar cap (Fig. 4a). We interpret this part of the response as that which projects onto the zonal mean of the geopotential response seen in Fig. 2b; it appears to be directly tied to the local enhancement of the lower-tropospheric baroclinicity by the snow perturbation. The significant Δ**F** signal is also located in the lower troposphere and exhibits weak upward and equatorward wave propagation away from the snow perturbation region (Fig. 4b).

The response intensifies during the growth phase and the waves propagate more poleward and penetrate into the lower stratosphere, causing a significant deceleration of the polar night jet (Figs. 4c,d). We also note a significant positive wind response in the subtropical stratosphere that is associated with an area of weak EP flux divergence. Convergence in Δ**F** occurs above 100 hPa and poleward of 40°N as the waves deposit their westward momentum, inducing a torque that decelerates the winds. The largest contribution to Δ**F** comes from zonal wavenumbers 1–3 (analysis not shown), demonstrating that the regional forcing can generate a planetary-scale response that penetrates into the stratosphere.

The mature phase is marked by a negative tropospheric NAM response in the winds (Fig. 4e), the sea level pressure (Fig. 2g), and the wave activity fluxes (Fig. 4f; cf. Fig. 6b of Limpasuvan and Hartmann 2000). We note the reflection of the wave activity pulse response back into the polar troposphere, the dipolar response of the winds, and the negative polar SLP response. Thus, we see over time the transition of the response from a thermally direct response in the onset phase to a dynamical annular mode response involving strong eddy forcing (Peng et al. 2003; Deser et al. 2007).

We examine the day-to-day evolution of the annular mode–type response by using the geopotential height averaged over the polar cap poleward of 60°N ($Z_{PC}$). The $n = 100$ ensemble mean response of $Z_{PC}$ to the snow forcing ($\Delta Z_{PC}$) is shown in Fig. 5 and is similar F5 when plotted for randomly sampled $n = 50$ subsets (not shown). During the onset phase, the most significant response is a tropospheric low centered at 400 hPa. The low persists through the growth phase until day 50 when the tropospheric response changes to a weak high, indicating anticyclonic circulation over the polar cap. The weak tropospheric high appears to lag behind a highly significant positive $\Delta Z_{PC}$ response in the lower stratosphere that begins during the growth phase around day 25. Positive $\Delta Z_{PC}$ signifies a warming of the polar stratosphere, which coincides with the intensification in Δ**F** (Fig. 4d), indicating a wave-driven disturbance to the polar vortex. In agreement with previous observational studies (Baldwin and Dunkerton 2001; Polvani and Waugh 2004; Cohen et al. 2007), this stratospheric circulation response progresses downward into the troposphere and a weaker like-signed anomaly reaches the surface, associated with a response in the zonal mean

JOBNAME: JCLI 21#21 2008 PAGE: 7 SESS: 8 OUTPUT: Sat Dec 6 06:24:49 2008 Total No. of Pages: 15
/ams/jcli/170147/jcli2505





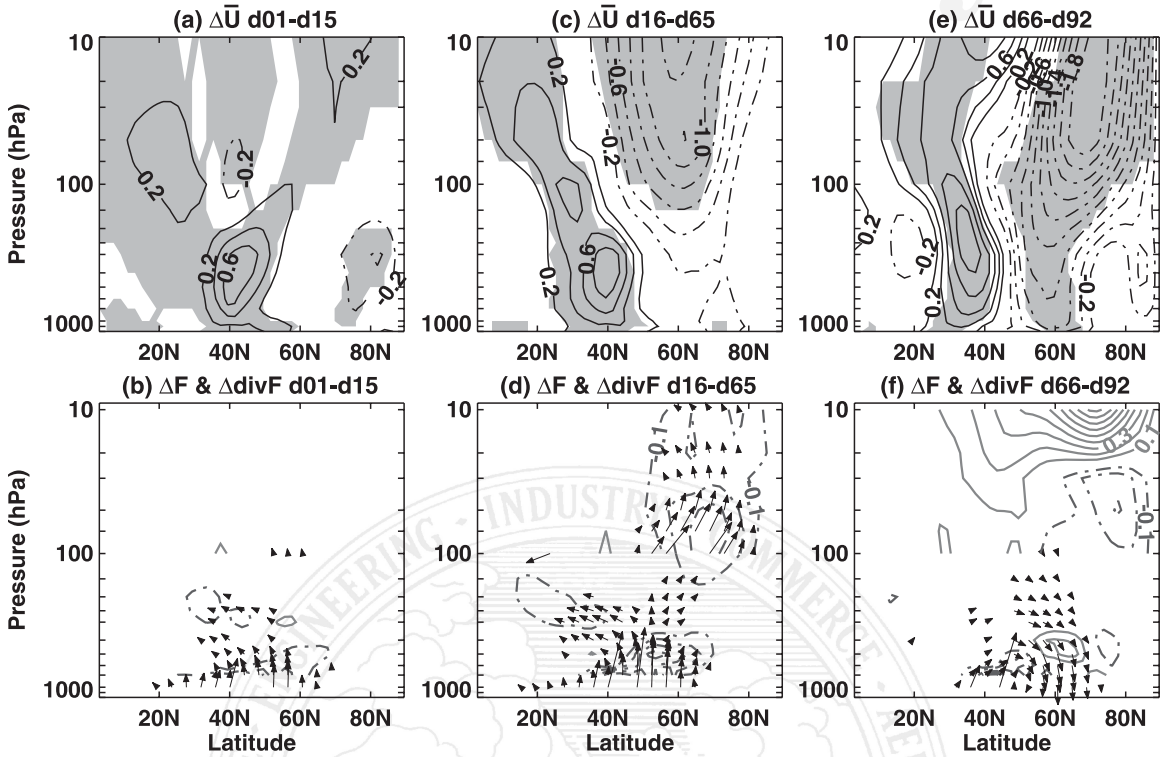


FIG. 4. As Fig. 2 except for (a), (c), (e) zonal mean zonal wind ($\Delta\bar{U}$), and (b), (d), (f) EP flux vectors ($\Delta\mathbf{F}$) and EP flux divergence $\Delta$div $\mathbf{F}$. Contour interval (a), (c), (e) is 0.2 m s$^{-1}$ and (b), (d), (f) is 0.2 m s$^{-1}$ day$^{-1}$ below 100 hPa and 0.1 m s$^{-1}$ day$^{-1}$ above 100 hPa. Longest meridional vector is $5 \times 10^6$ kg s$^{-2}$ below 100 hPa and $2 \times 10^5$ kg s$^{-2}$ above 100 hPa. Longest vertical vector is $3.5 \times 10^4$ kg s$^{-2}$ below 100 hPa and $4 \times 10^3$ kg s$^{-2}$ above 100 hPa.

geopotential that projects onto the negative NAM pattern (Fig. 5b).

In Fletcher et al. (2007), we found that those realizations for which the polar vortex was initially weak prior to the imposition of the snow perturbation displayed a significantly stronger positive anomaly in the troposphere. We will return to this point in section 4a.

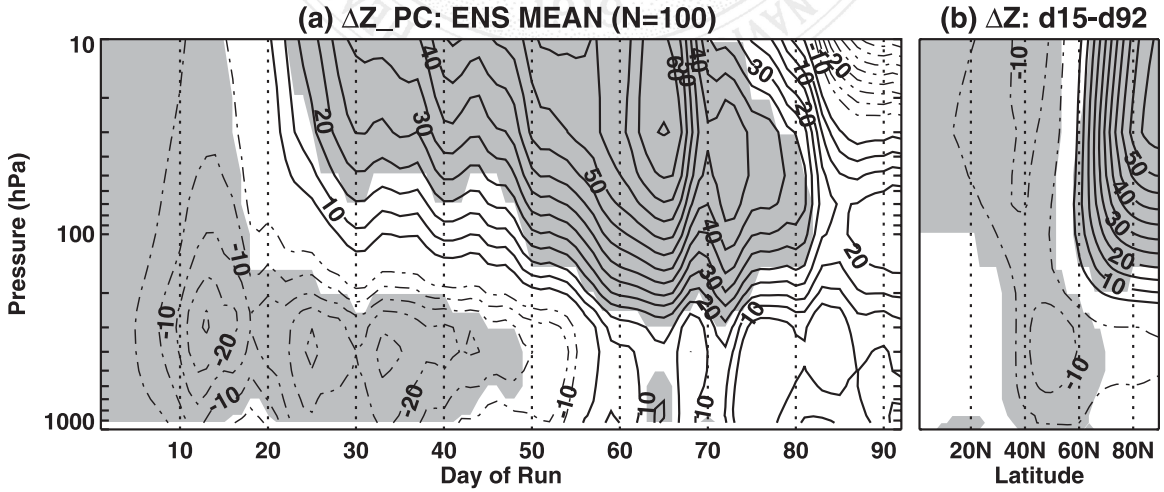


FIG. 5. (a) Time–pressure cross section of the ensemble mean $Z_{PC}$ response ($\Delta$Z_PC). Contour interval is 5 m and negative contours are dashed. Shading as in Fig. 2. (b) The zonal mean geopotential height response ($\Delta Z$) time averaged between days 15 and 92.Contours as in (a), and shading as in Fig. 2.

JOBNAME: JCLI 21#21 2008 PAGE: 8 SESS: 8 OUTPUT: Sat Dec 6 06:24:50 2008 Total No. of Pages: 15
/ams/jcli/170147/jcli2505





*b. Sensitivity to the perturbation*

Our experimental design is intended to represent, in a simple way, the impact on the atmosphere of a persistent snow extent anomaly over Siberia. We now test the response's sensitivity to the timing and persistence of the snow perturbation. We first test the sensitivity of the response to the timing of the snow perturbation by varying the snow switch-on date. In our original simulations (section 2b) the switch-on occurred on 1 October (hereafter OCT runs). In a second ensemble of simulations initialized from the same set of 100 independent initial conditions, we switch on the snow forcing 1 month later, on 1 November (hereafter NOV runs). Between 1 October and 1 November the HIGH-SNOW and LOW-SNOW branches in NOV are identical, with the snow mass fixed in both sets of simulations at its 1 October value.[1]

F6 Figure 6 shows various aspects of the response to the snow perturbation for the OCT (plotted with a solid curve) and the NOV (plotted with a dotted curve) cases, as a function of the time from switch-on of the forcing. (We will discuss the quantities represented by the dashed curve below.) The surface cooling over Siberia in NOV during days 1–30 is weaker than in OCT by around 1.5 K (Fig. 6a), which is caused directly by the seasonal cycle of insolation: less SW is available in November than in October, so the effect of increased surface albedo is reduced. However, the temperature responses converge after day 30 as the difference in available insolation between the OCT and NOV integrations is reduced.

To assess the sensitivity in the planetary wave response to the timing of the snow perturbation, in Fig. 6b we show the cumulative response in daily zonal mean eddy meridional heat flux $(\Sigma\Delta\overline{v'T'})$, which is roughly proportional to the vertical component of **F** (Andrews et al. 1987). The cumulative $\Delta\overline{v'T'}$ is relevant here because it has been shown that the zonal mean circulation responds to a buildup in **F**, rather than to the instantaneous wave driving (Newman et al. 2001; Polvani and Waugh 2004). Consistent with the reduced surface cooling, the peak $\Sigma\Delta\overline{v'T'}$ in NOV is weaker than in OCT, reaching around half the amplitude before decaying after 50 days. Interestingly, however, the cumulative absorption of wave activity by the polar stratosphere

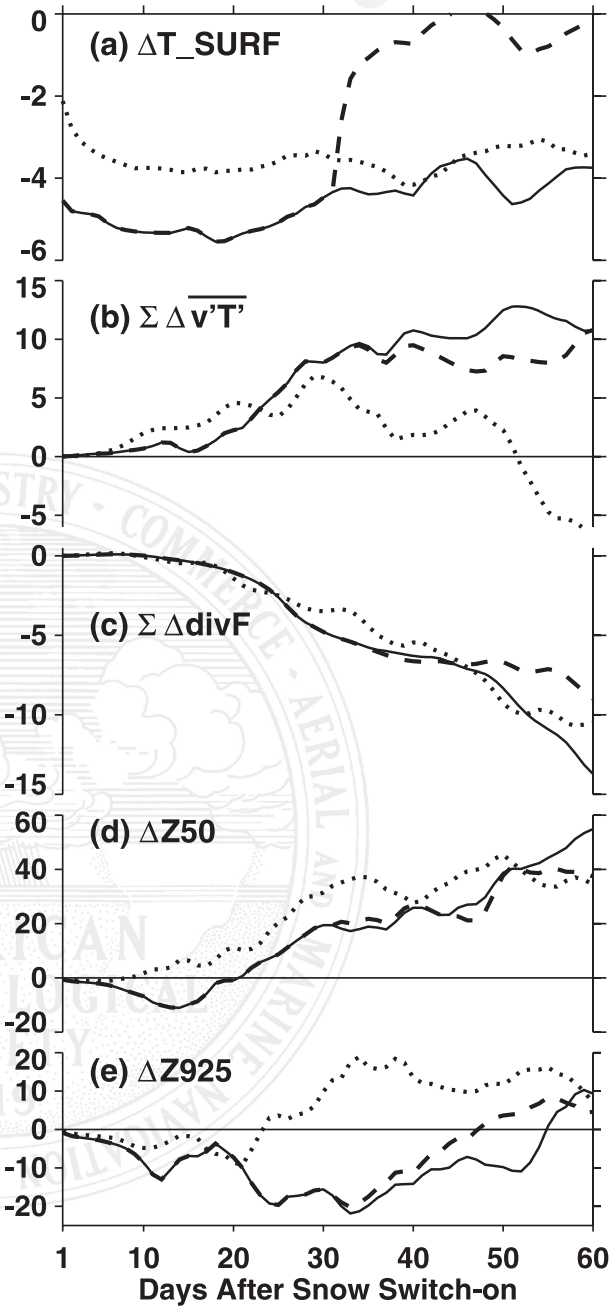


FIG. 6. The time evolution of the ensemble mean response following the switch-on of the snow perturbation in the OCT runs (solid lines), NOV runs (dotted lines), and OCT2 runs (dashed lines). (a) Area-average surface temperature response over Siberia (ΔT_SURF), (b) cumulative meridional heat flux response $(\Sigma\Delta\overline{v'T'})$ at 100 hPa averaged between 40° and 80°N, (c) cumulative EP flux divergence response ($\Sigma\Delta div$F) at 50 hPa averaged over the polar cap (poleward of 60°N), (d) geopotential height at 50 hPa area averaged over the polar cap ($\Delta Z50$), and (e) geopotential height at 925 hPa area averaged over the polar cap ($\Delta Z925$). Units are (a) K, (b) m K $s^{-1}$, (c) $m^3\ s^{-1}\ kg^{-1} \times 10^5$, and (d), (e) m. Abscissa shows the number of days after the snow perturbation switch-on date and not calendar day.

[1] From observations of snow cover extent (e.g., Robinson et al. 1993), October and November appear to be the only 2 months when Siberian snow forcing could lead to significant interannual variations of the boreal winter NAM. September is a relatively warm month with little snow and December is cold with almost complete snow coverage and with relatively little insolation. We therefore would expect little interannual variability in snow extent and snow-forced diabatic cooling in these months.

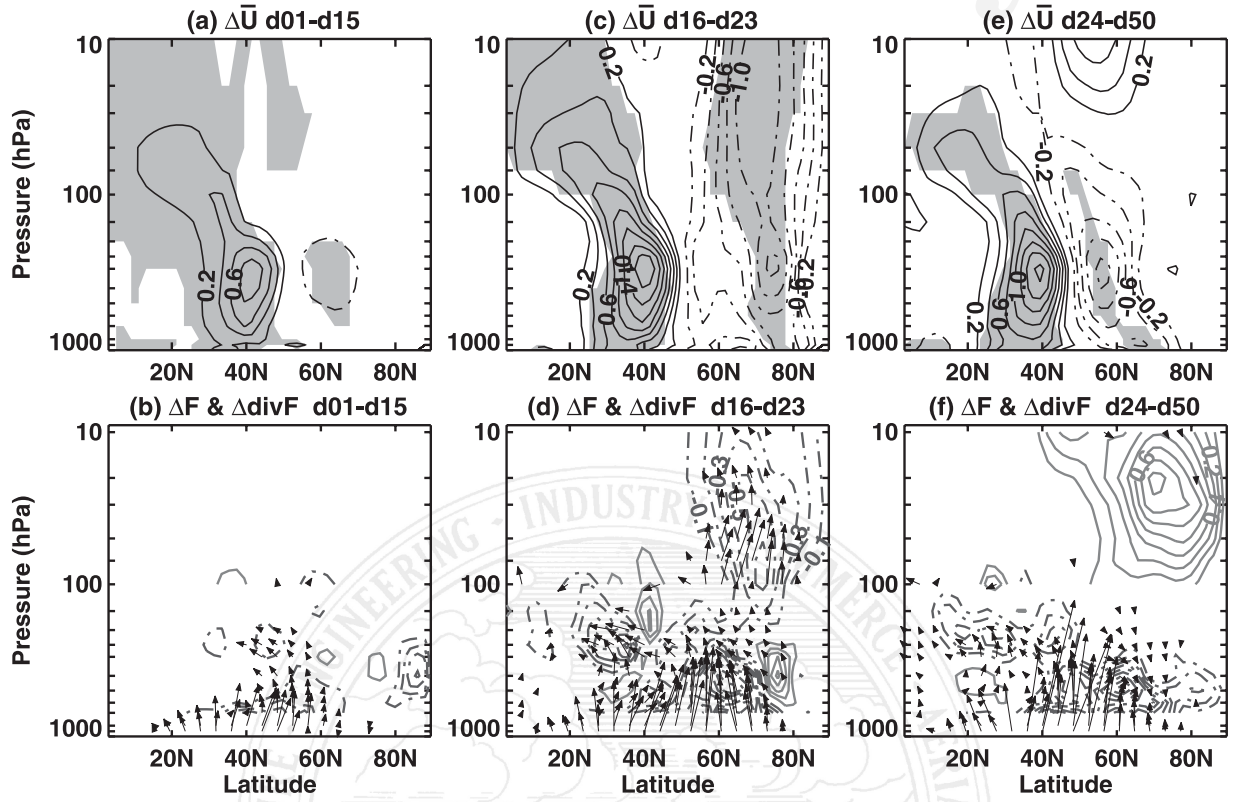


FIG. 7. Same as Fig. 4, except for the AM2-HI model and time averaging periods (a), (b) days 1–15, (c), (d) days 16–23, and (e), (f) days 24–50.

(ΣΔdiv **F**, Fig. 6c) evolves similarly in OCT and NOV. This suggests that the available wave activity is absorbed more efficiently by the stratosphere in November than in October, perhaps because the stronger westerly jet in November provides a more efficient guide for the upward-propagating wave activity (see also Fig. 11). The similarity in the absorption of wave activity results in a circulation response in the polar stratosphere in NOV that is comparable to OCT (Fig. 6d). In the lower troposphere the high polar cap geopotential response in NOV achieves a similar peak amplitude to OCT, however, it becomes positive after just 25 days in NOV compared to 55 days in OCT (Fig. 6e). The positive geopotential response in NOV occurs ~10 days after the peak in $\Sigma\Delta\overline{v'T'}$, indicating a more rapid progression of the response from the stratosphere into the troposphere than in OCT.

We next test the sensitivity of the response to the persistence of the snow perturbation by varying the duration of the forcing. In particular, we carry out a third ensemble of simulations (hereafter OCT2 runs) in which the snow perturbation is switched off on 1 November, 1 month after switch-on. That is, on 1 November each realization has its snow mass over Siberia returned from the perturbed value to its 1 October value. This experiment is intended to represent the impact of a large fall season snowfall event that does not persist into winter.

The dashed curves in Fig. 6 show the results from the OCT2 runs, which diverge from the OCT runs after the snow switch-off date (day 32). Following the switch-off, the surface temperature response quickly reduces to almost zero (Fig. 6a). Around 5–10 days later, the cumulative wave activity response in OCT2 flattens out, but absorption of wave activity continues in the polar stratosphere, albeit at a reduced rate (Figs. 6b,c). Switching off the snow perturbation after 1 month has little impact on the circulation response (Figs. 6d,e), which demonstrates the potential for a time-lagged circulation response to snowfall anomalies more like that seen in observations (Cohen et al. 2007). Analysis of the sensitivity to the duration and timing of the forcing using simpler dynamical models is ongoing.

## 4. Impact of stratospheric representation

### *a. Response to snow forcing*

The robustness of the response to changes in the timing and duration of the snow forcing shows how the

JOBNAME: JCLI 21#21 2008 PAGE: 10 SESS: 8 OUTPUT: Sat Dec 6 06:24:52 2008 Total No. of Pages: 15
/ams/jcli/170147/jcli2505





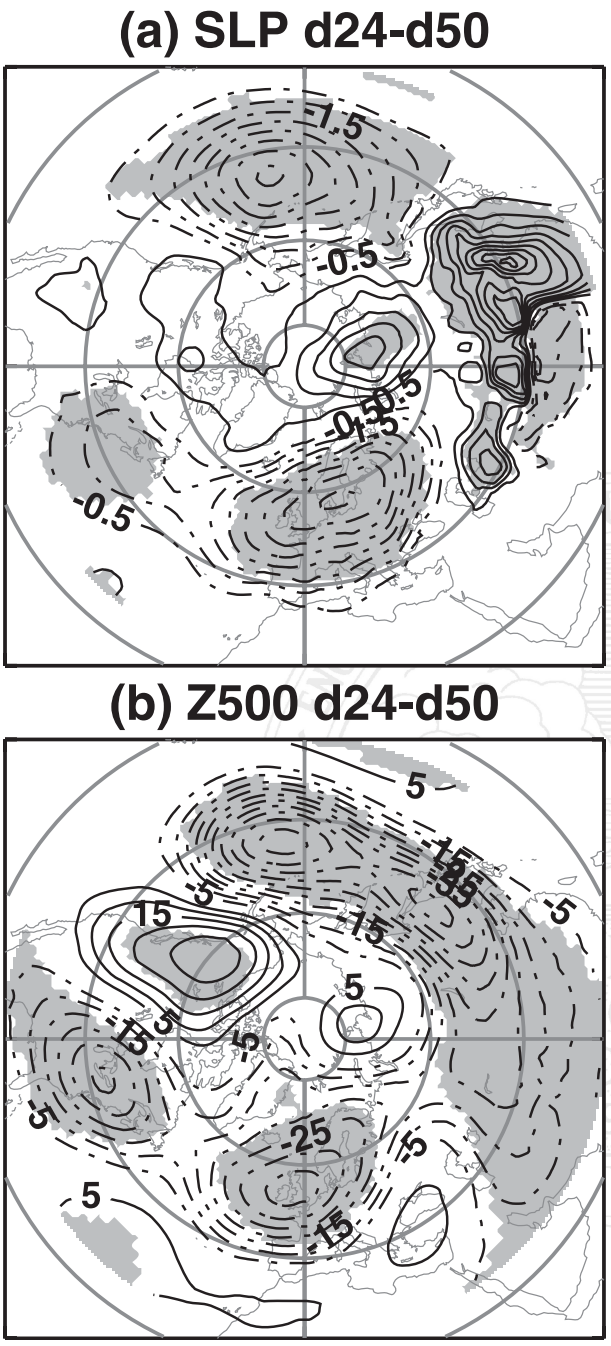


FIG. 8. (a) and (b) Same as Figs. 2g,h, except for the AM2-HI model.

relatively long time scale in the stratosphere might provide memory to the climate system: once the stratospheric mean flow is perturbed by a wave driving event the response can persist even if the snow and wave driving do not. Given the important role for the stratosphere emphasized in previous work on the topic, we next examine the sensitivity of the response to stratospheric representation by repeating the snow-forcing GCM ensemble with the AM2-HI model described in section 2a. In particular, we have branched 100 pairs of HIGH-SNOW and LOW-SNOW runs from a 100-yr control integration performed with AM2-HI. As we demonstrate, the high-top/low-top comparison sheds light on which aspects are sensitive to stratospheric representation.

Although the tropospheric onset phase of the response to snow forcing is similar in AM2-LO and AM2-HI, there is a striking acceleration and weakening of the part of the response involving wave-mean flow interactions in AM2-HI. While in AM2-LO the growth and mature phase of the response, seen in Fig. 4, persists for up to 12 weeks, the corresponding phases persist for only about 4 weeks in AM2-HI. This is shown in Fig. 7, F7 which plots the zonal wind and wave driving response for the AM2-HI model. In addition to the reduced duration of the growth and mature phases, another notable difference is that the response in the polar stratospheric winds is less persistent in AM2-HI than in AM2-LO. By days 24–50 the polar night jet in AM2-HI has relaxed back to its climatological value, while the dipole response in the lower-tropospheric winds that projects onto a negative NAM pattern remains in place (Fig. 7e). Therefore, while the response pattern in the lower troposphere is similar between AM2-LO and AM2-HI, the major difference is that in AM2-HI the stratospheric part persists for roughly one-third as long. Finally, in Fig. 8 we show the equivalent to Fig. 2 but for AM2-HI F8 during the mature stage only. This reinforces the point that the tropospheric response in AM2-HI closely resembles that in AM2-LO in SLP and geopotential height but this pattern does not persist beyond day 50.

In Fig. 9, which shows the day-to-day evolution of F9 $\Delta Z_{PC}$ in AM2-HI for days 1–50 and should be compared to Fig. 5, we see a response that is similar at the onset but diverges after day 15. The stratospheric response is again a warming, but a relatively weak one whose downward propagation occurs relatively quickly but barely penetrates into the troposphere. After about day 45 no further systematic response is seen in either the troposphere or stratosphere, as measured by our significance tests.

In Fletcher et al. (2007) we have shown that the strength of the stratosphere–troposphere response to snow is strongly controlled by the initial state of the stratosphere in the AM2-LO model. We carry out a similar analysis here with the high-top and low-top models. In particular, we compare the response for those realizations with axpolar vortex that is initially weak ($Z_{PC(10hPa)} > 0$ for the week prior to the perturbation) to those with a polar vortex that is initially strong ($Z_{PC(10hPa)} < 0$ for the

JOBNAME: JCLI 21#21 2008 PAGE: 11 SESS: 8 OUTPUT: Sat Dec 6 06:24:55 2008 Total No. of Pages: 15
/ams/jcli/170147/jcli2505





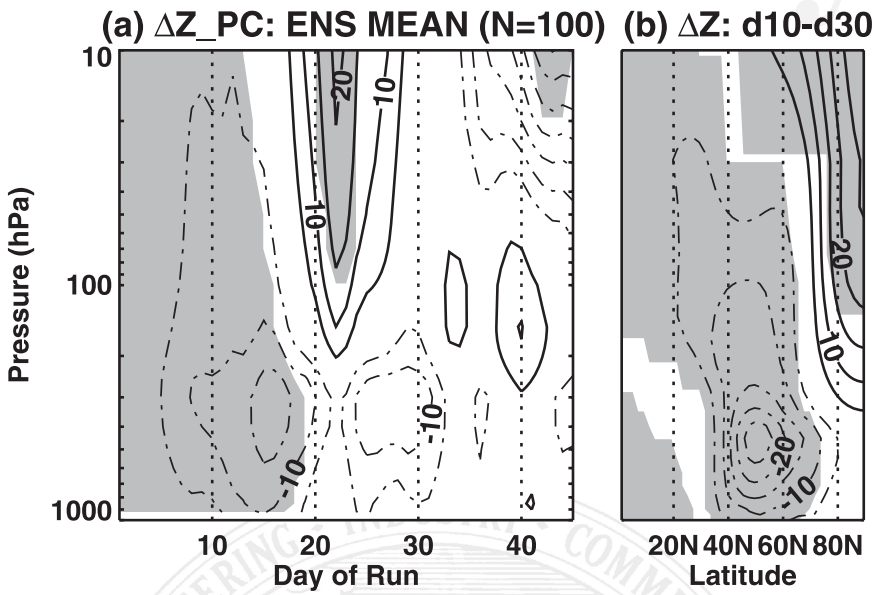


FIG. 9. Same as Fig. 5, except for the AM2-HI model, (a) shows days 1–45 only and (b) shows time average for days 10–30.

week prior). We show the ensemble mean $\Delta Z_{PC}$ separately for the weak and strong initial polar vortex cases and for the AM2-HI and AM2-LO models in Fig. 10. In both AM2-LO and AM2-HI the tropospheric response becomes more positive after 2 weeks in the weak vortex cases; and the tropospheric response remains more negative for longer in the strong vortex cases. These results, which are consistent with Fletcher et al. (2007),

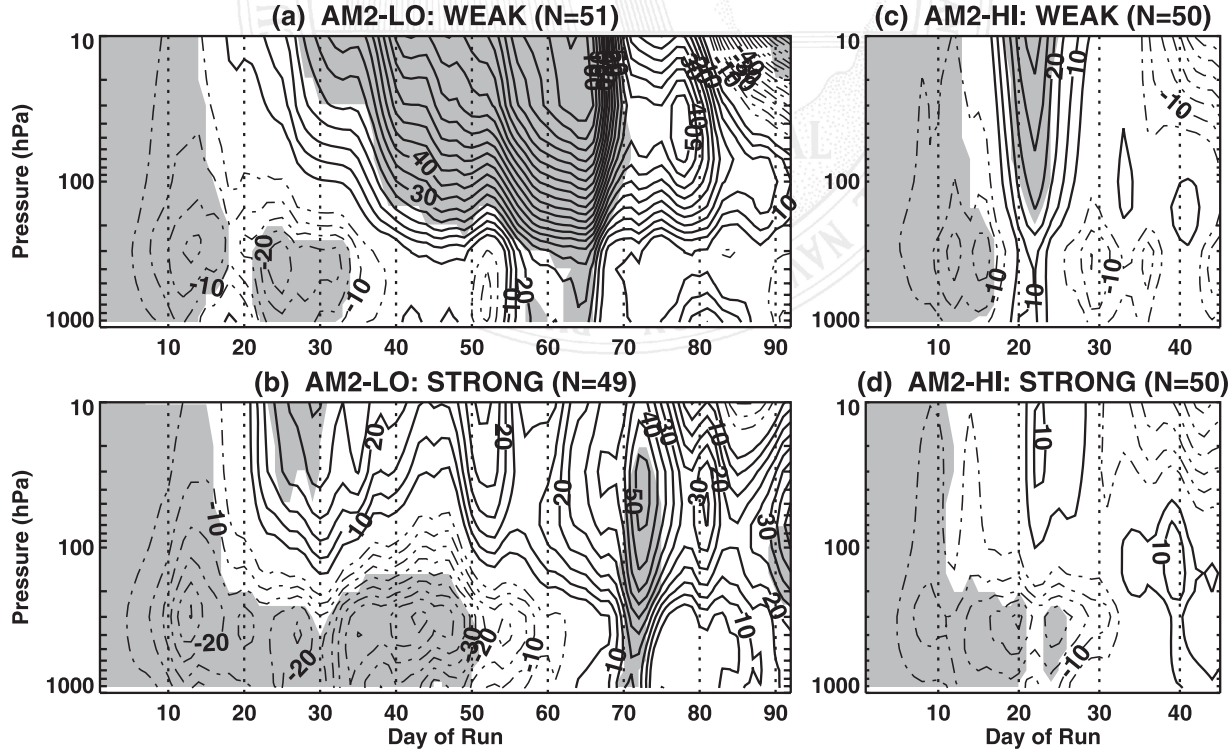


FIG. 10. (a), (b) Same as Fig. 5a, and (c) and (d) same as Fig. 9a except composited for cases with (a), (c) an initially weak or (b), (d) an initially strong polar vortex in the week prior to imposing the snow perturbation.

JOBNAME: JCLI 21#21 2008 PAGE: 12 SESS: 8 OUTPUT: Sat Dec 6 06:24:57 2008 Total No. of Pages: 15
/ams/jcli/170147/jcli2505





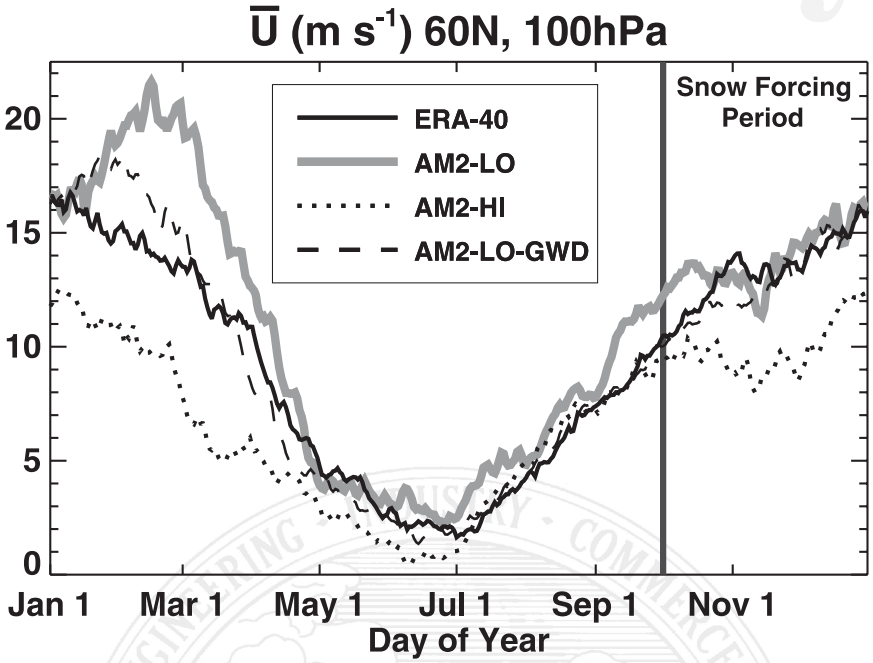


FIG. 11. Seasonal cycle of daily climatological zonal mean zonal wind at 60°N, 100 hPa ($\bar{U}$), in m s$^{-1}$ from ERA-40 (black solid line), AM2-LO (thicker gray line), AM2-HI (dotted line), and AM2-LO-GWD (dashed line). Thick vertical line indicates the start of the snow-forcing period (1 October), which ends on 31 December.

show that the control of the response by the stratospheric state is robust to changes in stratospheric representation. However, the AM2-HI response is clearly less persistent and weaker overall.

### b. *Causes of intermodel differences*

We next propose two explanations for why the response to snow forcing in AM2-HI is weaker and less persistent than in AM2-LO. First, Sigmond et al. (2008) and others have argued that the lower stratosphere is a particularly important region for controlling the amplitude and direction of the propagation of planetary waves from the troposphere into the stratosphere. Because our snow forcing has a lower-tropospheric origin, it is critical that the lower-stratospheric circulation is accurately simulated in order to obtain a realistic response.

Compared to 40-yr European Centre for Medium-Range Weather Forecasts (ECMWF) Re-Analysis (ERA-40) data (Uppala et al. 2005), Fig. 11 shows that AM2-LO is more realistic than AM2-HI in representing the seasonal cycle of lower-stratospheric zonal winds during the snow-forcing period. The winds in AM2-HI are much too weak, which through the Charney–Drazin criterion (Charney and Drazin 1961) reduces the possibility for planetary waves to propagate into the stratosphere. A complete explanation of the differences between AM2-HI and AM2-LO is beyond the scope of this study. However, we have found that the differences cannot be accounted for simply by the change in upper-level dissipation described in section 2a. To demonstrate this, Fig. 11 also shows the winds from an unforced control run of AM2-LO-GWD, which consists of AM2-LO with the Rayleigh drag scheme replaced by the Alexander–Dunkerton (Alexander and Dunkerton 1999) nonorographic GWD scheme with the settings of AM2-HI. The presence of the nonorographic GWD scheme has little impact on the winds in this region. However, we do find (not shown) substantial differences between AM2-LO and AM2-LO-GWD in the circulation outside of the polar regions. We therefore determine that a combination of the vertical resolution and the different treatment of unresolved waves is the cause of the differences in the winds and planetary waves between AM2-LO and AM2-HI.

Second, recent work has shown that time scales of variability in the stratosphere exert a strong control on stratosphere–troposphere coupling (Norton 2003; Baldwin et al. 2003) and on forcing/response simulations (Gerber et al. 2008; Ring and Plumb 2007). We here find evidence for a similar type of control. In Fig. 12, we plot the decorrelation time scale statistic ($\tau$) for 1 October–31 December daily polar cap mean geopotential heights for the ERA-40 and for the unforced control runs of our

JOBNAME: JCLI 21#21 2008 PAGE: 13 SESS: 8 OUTPUT: Sat Dec 6 06:24:58 2008 Total No. of Pages: 15
/ams/jcli/170147/jcli2505





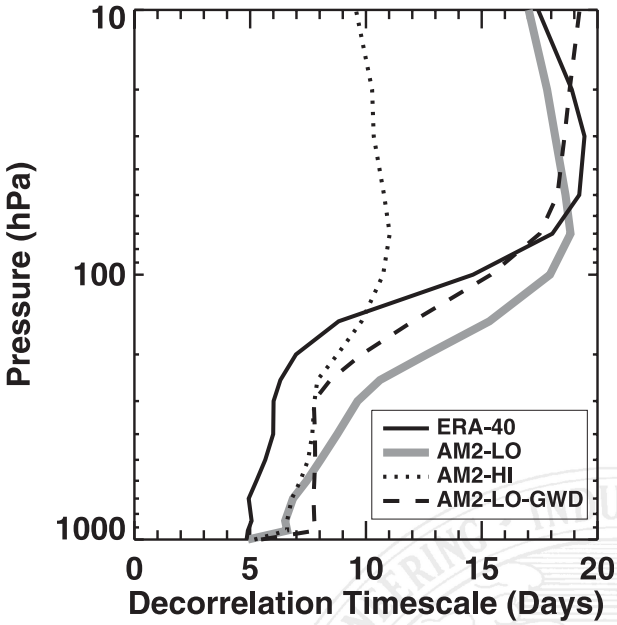


FIG. 12. The decorrelation time scale statistic ($\tau$) in days at each pressure level for 1 October–31 December daily polar cap–averaged geopotential height. Line definitions and styles are as in Fig. 11.

AM2 simulations. Following Gerber et al. (2008), the $\tau$ statistic is extracted from a linear least squares fit of log $[Z_{PC}(t)]$ to time at each pressure level. In the reanalysis, $\tau$ increases from about 5–6 days in the troposphere to about 17–20 days in the stratosphere. AM2-LO and AM2-LO-GWD are somewhat more persistent in the troposphere but generally exhibit similar behavior; however, $\tau$ in the AM2-HI stratosphere is about half of that in AM2-LO, AM2-LO GWD, and reanalysis data. Thus, circulation anomalies in AM2-HI are damped on an unrealistically fast time scale compared to the two low-top GCMs.

There are certain aspects of the high-top/low-top comparison that are more ambiguous, particularly in the region above the lower stratosphere (above 50 hPa). In this region the winds in AM2-LO are significantly stronger than the reanalysis data, while the winds in AM2-HI are weaker than the reanalysis data. However, AM2-LO cannot be expected to properly resolve this part of the circulation because it has very coarse vertical resolution above 50 hPa, and its circulation anomalies are damped artificially by the Rayleigh drag sponge layer. The weak winds in AM2-HI are partially explained through stronger climatological planetary wave activity (relative to AM2-LO), however, other factors probably also play a role because the wave activity in AM2-HI is actually weaker than in reanalysis data. Therefore, certain aspects of the AM2-HI model we cannot fully explain and are the subject of ongoing investigation.

Our overall conclusion is, based on the unforced climatologies in the critical lower-stratospheric region, that the AM2-LO model has a more realistic circulation than AM2-HI and is therefore more appropriate for the snow-forcing experiments. We have carried out an additional ensemble of snow-forcing integrations with AM2-LO GWD to further test this hypothesis. The amplitude and timing of the response to snow forcing in AM2-LO GWD is similar to that of AM2-LO (not shown). Further work with a suite of additional models will help elucidate this issue.

## 5. Conclusions

This study in several ways extends the Gong et al. (2003) analysis, which examines the response to Siberian snow perturbations in a 20-member ensemble using the (low top) ECHAM3 model. First, we here use a simpler snow-forcing perturbation that we hope will be easy to reproduce in other models, thus allowing for clean intercomparisons for this important seasonal prediction problem. Second, we have greatly increased the number of realizations, because we found that the ensemble mean response did not converge with fewer than 50 realizations. Having the full set of 100 realizations on hand allowed us to try to explain the spread in the response (see Fletcher et al. 2007; Fig. 10 in this paper); this has lead to new insights on stratospheric control of the response to snow forcing. Third, we have compared two versions of the relatively new GFDL AM2 model with and without a well-resolved stratosphere. We have carried out extensive robustness tests to the timing of the forcing, to stratospheric representation, and to upper-layer dissipation. While our basic results are consistent with those of Gong et al. (2003) our main contribution has been to provide more insight into the dynamical aspects of the response.

We summarize our main conclusions as follows:

- Fall season snow perturbations in the Eurasian sector can give rise to a robust teleconnected response in the stratosphere and troposphere. The response in the growth phase is related to a tropospheric form stress anomaly associated with vertical propagation of wave activity. The surface forcing is capable of generating significant negative NAM anomalies in the stratosphere that can subsequently propagate downward; that is, snow forcing can lead to Baldwin and Dunkerton (2001)-type events in the stratosphere–troposphere system.
- The timing and amplitude of the response represented in AM2-LO is robust to changes in the onset

time of the perturbation. Thus, although this study was motivated by the October snow-forcing problem, the basic mechanism is also observed with a November snow forcing and is also not tied to persistence of the snow perturbation.

- The persistence and amplitude of the stratosphere–troposphere response, particularly in the mature phase, is highly sensitive to stratospheric representation.

Our results leave important questions unanswered. The first concerns the realism of the snow–atmosphere coupling represented in the GCM. We have shown that the persistence and amplitude of the response to the snow forcing can be controlled by model details. However, even robust aspects of the simulated response do not always correspond to observed circulation anomalies associated with October snow forcing. For example, the polar tropospheric low seen in the onset and growth phase of the response is not seen in observations (e.g., Cohen et al. 2007), and we have no simple explanation for this.

More generally, we know that this GCM, as is the case for many other GCMs, is incapable of spontaneously AU1 simulating observed snow variability (Frei et al. 1999, 2003). We have investigated snow–atmosphere coupling in a variety of GCMs and find that the snow-forced stratosphere–troposphere coupling events documented in Cohen et al. 2007 are poorly simulated in control simulations of many models (Hardiman et al. 2008). The cause of this lack of realism is unclear, but this, in fact, is why we in this study must stimulate such events by imposing large-scale snow anomalies in models.

Second, there is the question of the role of the stratosphere and of stratospheric representation in controlling the response to snow and other types of tropospheric forcing. Many hypotheses have been put forward on stratospheric control (see, e.g., Perlwitz and Harnik 2003; Norton 2003; Limpasuvan et al. 2004; Gerber et al. 2008; Ring and Plumb 2007). We have argued that the key controls are the strength of the lower-stratospheric zonal wind and the time scale of damping of stratospheric anomalies, but this claim has still to be investigated in detail and tested against the alternate hypothesis that the parameterization of unresolved waves is responsible for altering the response to the tropospheric snow-forced wave activity pulse. To obtain clear results, testing along the lines of the strategy outlined in Sigmond et al. (2008) and with simplified models will probably be required.

*Acknowledgments.* CGF and PJK acknowledge support from the Canadian Foundation for Climate and Atmospheric Sciences Grant 506. SCH is supported by the Natural Sciences and Engineering Research Council of Canada. JC was supported by NSF Grant ATM-0443512. We thank GFDL for the model code and technical support and Dr. Sabine Stanley for providing computational resources. The AM2-HI and AM2-LO GWD simulations were performed on the Sunnyvale cluster at the Canadian Institute for Theoretical Astrophysics. We thank three anonymous reviewers for their helpful comments.

## REFERENCES

Alexander, M. J., and T. J. Dunkerton, 1999: A spectral parameterization of mean-flow forcing due to breaking gravity waves. *J. Atmos. Sci.,* **56,** 4167–4182.

Anderson, J., and Coauthors, 2004: The new GFDL global atmosphere and land model AM2–LM2: Evaluation with prescribed SST simulations. *J. Climate,* **17,** 4641–4673.

Andrews, D. G., J. R. Holton, and C. B. Levoy, 1987: *Middle Atmosphere Dynamics.* Academic Press, 489 pp.

Austin, J., and R. J. Wilson, 2006: Ensemble simulations of the decline and recovery of stratospheric ozone. *J. Geophys. Res.,* **111,** D16314, doi:10.1029/2005JD006907.

Baldwin, M. P., and T. P. Dunkerton, 2001: Stratospheric harbingers of anomalous weather regimes. *Science,* **294,** 581–584.

——, D. B. Stephenson, D. W. J. Thompson, T. J. Dunkerton, A. J. Charlton, and A. O'Neill, 2003: Stratospheric memory and skill of extended-range weather forecasts. *Science,* **301,** 636–640.

Charlton, A. J., A. O'Neill, W. Lahoz, A. Massacand, and P. Berrisford, 2004: Sensitivity of tropospheric forecasts to stratospheric initial conditions in both hemispheres. *Quart. J. Roy. Meteor. Soc.,* **130,** 1771–1792.

Charney, J. G., and P. G. Drazin, 1961: Propagation of planetary-scale disturbances from lower into upper atmosphere. *J. Geophys. Res.,* **66,** 83–109.

Cohen, J., and D. Rind, 1991: The effect of snow cover on the climate. *J. Climate,* **4,** 689–706.

——, and D. Entekhabi, 1999: Eurasian snow cover variability and Northern Hemisphere climate predictability. *Geophys. Res. Lett.,* **26,** 345–348.

——, and C. Fletcher, 2007: Improved skill of Northern Hemisphere winter surface temperature predictions based on land–atmosphere fall anomalies. *J. Climate,* **20,** 4118–4132.

——, M. Barlow, P. J. Kushner, and K. Saito, 2007: Stratosphere–troposphere coupling and links with Eurasian land surface variability. *J. Climate,* **20,** 5335–5343.

Delworth, T. L., and Coauthors, 2006: GFDL's CM2 global coupled climate models. Part I: Formulation and simulation characteristics. *J. Climate,* **19,** 643–674.

Deser, C., R. A. Tomas, and S. Peng, 2007: The transient atmospheric circulation response to North Atlantic SST and sea ice anomalies. *J. Climate,* **20,** 4751–4767.

Fletcher, C. G., P. J. Kushner, and J. Cohen, 2007: Stratospheric control of the extratropical circulation response to surface forcing. *Geophys. Res. Lett.,* **34,** L21802, doi:10.1029/2007GL031626.

Frei, A., and D. A. Robinson, 1998: Evaluation of snow extent and its variability in the Atmospheric Model Intercomparison Project. *J. Geophys. Res.,* **103,** 8859–8871. AU2

——, J. A. Miller, and D. A. Robinson, 2003: Improved simulations of snow extent in the second phase of the Atmospheric Model Intercomparison Project (AMIP-2). *J. Geophys. Res.,* **108,** 4369, doi:10.1029/2002JD003030.

Gerber, E. J., S. Voronin, and L. M. Polvani, 2008: Testing the annular mode autocorrelation time scale in simple atmospheric general circulation models. *Mon. Wea. Rev.,* **136,** 1523–1536.

Gong, G., D. Entekhabi, and J. Cohen, 2003: Modeled Northern Hemisphere winter climate response to realistic Siberian snow anomalies. *J. Climate,* **16,** 3917–3931.

Hardiman, S. C., P. J. Kushner, and J. Cohen, 2008: Investigating the effect of fall Eurasian snow cover on winter climate in General Circulation Models. *J. Geophys. Res.,* **113,** D21123, doi:10.1029/2008JD010623.

Holton, J. R., 2004: *An Introduction to Dynamic Meteorology*. Academic Press, 535 pp.

Hoskins, B. J., and D. Karoly, 1981: The steady linear response of a spherical atmosphere to thermal and orographic forcing. *J. Atmos. Sci.,* **38,** 1179–1196.

Kushner, P., and Coauthors, 2007: The SPARC DynVar project: A SPARC project on the dynamics and variability of the coupled stratosphere-troposphere system. *SPARC Newsletter,* No. 29, World Climate Research Programme, 9–14.

Kushnir, Y., W. Robinson, P. Chang, and A. Robertson, 2006: The physical basis for predicting Atlantic sector seasonal-to-interannual climate variability. *J. Climate,* **19,** 5949–5970.

Limpasuvan, V., and D. Hartmann, 2000: Wave-maintained annular modes of climate variability. *J. Climate,* **13,** 4414–4429.

——, D. W. J. Thompson, and D. L. Hartmann, 2004: The life cycle of the Northern Hemisphere sudden stratospheric warmings. *J. Climate,* **17,** 2584–2596.

——, D. L. Hartmann, D. W. J. Thompson, K. Jeev, and Y. L. Yung, 2005: Stratosphere-troposphere evolution during polar vortex intensification. *J. Geophys. Res.,* **110,** D24101, doi:10.1029/2005JD006302.

Lin, S. J., 2004: A ''vertically Lagrangian'' finite-volume dynamical core for global models. *Mon. Wea. Rev.,* **132,** 2293–2307.

Newman, P. A., E. R. Nash, and J. E. Rosenfield, 2001: What controls the temperature of the Arctic stratosphere during the spring? *J. Geophys. Res.,* **106** (D17), 19 999–20 010.

Norton, W. A., 2003: Sensitivity of Northern Hemisphere surface climate to simulation of the stratospheric polar vortex. *Geophys. Res. Lett.,* **30,** 1627, doi:10.1029/2003GL016958.

Panagiotopoulos, F., M. Shahgedanova, A. Hannachi, and D. B. Stephenson, 2005: Observed trends and teleconnections of the Siberian high: A recently declining center of action. *J. Climate,* **18,** 1411–1422.

Peng, S., W. A. Robinson, and S. Li, 2003: Mechanisms for the NAO response to the North Atlantic tripole. *J. Climate,* **16,** 1987–2004.

Perlwitz, J., and N. Harnik, 2003: Observational evidence of a stratospheric influence on the troposphere by planetary wave reflection. *J. Climate,* **16,** 3011–3026.

Polvani, L. M., and D. W. Waugh, 2004: Upward wave activity flux as a precursor to extreme stratospheric events and subsequent anomalous surface weather regimes. *J. Climate,* **17,** 3548–3554.

Ring, M. J., and R. A. Plumb, 2007: Forced annular mode patterns in a simple atmospheric general circulation model. *J. Atmos. Sci.,* **64,** 3611–3626.

Robinson, D. A., K. F. Dewey, and R. R. Heim, 1993: Global snow cover monitoring: An update. *Bull. Amer. Meteor. Soc.,* **74,** 1689–1696.

Shepherd, T. G., and T. A. Shaw, 2004: The angular momentum constraint on climate sensitivity and downward influence in the middle atmosphere. *J. Atmos. Sci.,* **61,** 2899–2908.

——, K. Semeniuk, and J. N. Koshyk, 1996: Sponge layer feedbacks in middle-atmosphere models. *J. Geophys. Res.,* **101** (D18), 23 447–23 464.

Siegmund, P., 2005: Stratospheric polar cap mean height and temperature as extended-range weather predictors. *Mon. Wea. Rev.,* **133,** 2436–2448.

Sigmond, M., J. F. Scinocca, and P. J. Kushner, 2008: Impact of the stratosphere on tropospheric climate change. *Geophys. Res. Lett.,* **35,** L12706, doi:10.1029/2008GL033573.

Thompson, D. W. J., and J. M. Wallace, 2000: Annular modes in the extratropical circulation. Part I: Month-to-month variability. *J. Climate,* **13,** 1000–1016.

Uppala, S. M., and Coauthors, 2005: The ERA-40 Re-analysis. *Quart. J. Roy. Meteor. Soc.,* **131,** 2961–3012.

Vallis, G. K., 2006: *Atmospheric and Oceanic Fluid Dynamics*. Cambridge University Press, 745 pp.

Vavrus, S., 2007: The role of terrestrial snow cover in the climate system. *Climate Dyn.,* **29,** 73–88.

Wilks, D. S., 2006: *Statistical Methods in the Atmospheric Sciences*. Academic Press, 648 pp.